

640x512 Pixel Four-Band, Broad-Band, and Narrow-Band Quantum Well Infrared Photodetector Focal Plane Arrays

S. D. Gunapala, S. V. Bandara, J. K. Liu, S. B. Rafol, C. A. Shott*, R. Jones*, S. Laband*, J. Woolaway II*, J. M. Fastenau**, A. K. Liu**, M. Jhabvala⁺, and K. K. Choi⁺⁺

Jet Propulsion Laboratory, California Institute of Technology
4800 Oak Grove Drive, Pasadena, CA 91109

*Indigo Systems Corporation, Santa Barbara, CA 93111

**IQE Inc., Bethlehem, PA 18015

⁺NASA Goddard Space Flight Center, Greenbelt, MD 20771

⁺⁺Army research Laboratory, Adelphi, MD 20783

ABSTRACT

A 9 μm cutoff 640x512 pixel hand-held quantum well infrared photodetector (QWIP) camera has been demonstrated with excellent imagery. Based on the single pixel test data, a noise equivalent differential temperature (NETD) of 8 mK is expected at 65K operating temperature with $f/2$ optics at 300K background. This focal plane array has shown background limited performance (BPLI) at 72K operating temperature with the same optics and background conditions. In this paper, we discuss the development of this very sensitive long wavelength infrared (LWIR) camera based on a GaAs/AlGaAs QWIP focal plane array and its performance in quantum efficiency, NETD, uniformity, and operability.

Key Words: Focal Plane Arrays, QWIPs, Long-wavelength Infrared (LWIR), Hand-held Camera

1. INTRODUCTION

A quantum well designed to detect infrared (IR) light is called a quantum well infrared photodetector (QWIP). An elegant candidate for QWIP is the square quantum well of basic quantum mechanics [1]. When the quantum well is sufficiently deep and narrow, its energy states are quantized (discrete). The potential depth and width of the well can be adjusted so that it holds only two energy states: a ground state near the well bottom, and a first excited state near the well top. A photon striking the well will excite an electron in the ground state to the first excited state, then an externally-applied voltage sweeps it out producing a photocurrent (Fig. 1). Only photons having energies corresponding to the energy separation between the two states are absorbed, resulting in a detector with a sharp absorption spectrum. Designing a quantum well to detect light of a particular wavelength becomes a simple matter of tailoring the potential depth and width of the well to produce two states separated by the desired photon energy. The GaAs/Al_xGa_{1-x}As material system allows the quantum well shape to be tweaked over a range wide enough to enable light detection at wavelengths longer than $\sim 6 \mu\text{m}$. Fabricated entirely

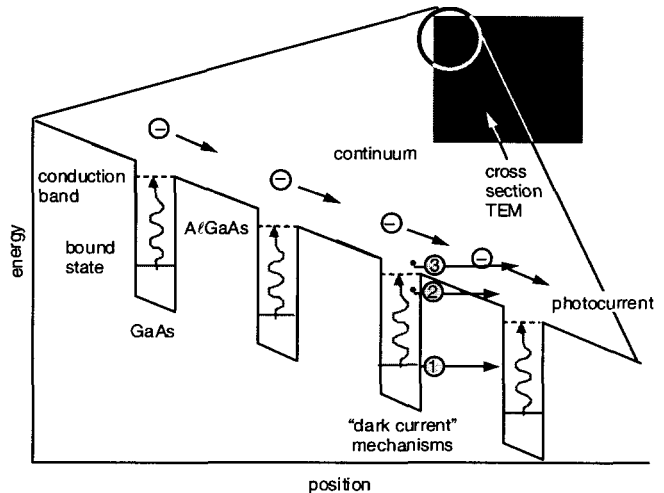


Fig. 1: Schematic diagram of the conduction band in a bound-to-quasibound QWIP in an externally applied electric field. Absorption of IR photons can photoexcite electrons from the ground state of the quantum well into the continuum, causing a photocurrent. Three dark current mechanisms are also shown: ground state tunneling (1); thermally assisted tunneling (2); and thermionic emission (3). The inset shows a cross-section transmission electron micrograph of a QWIP sample.

from large bandgap materials which are easy to grow and process, it is now possible to obtain large uniform FPAs of QWIPs tuned to detect light at wavelengths from 6 to 25 μm in the GaAs/ $\text{Al}_x\text{Ga}_{1-x}\text{As}$ material system [2-5].

Improving QWIP performance depends largely on minimizing the parasitic current that plagues all light detectors, the dark current (the current that flows through a biased detector in the dark, i.e., with no photons impinging on it). As we have discussed elsewhere [5], at temperatures above 45 K, the dark current of the QWIP is entirely dominated by classic thermionic emission of ground state electrons directly out of the well into the energy continuum. Minimizing this last component is critical to the commercial success of the QWIP as it allows the highly-desirable high-temperature camera operation.

Therefore, we have designed the *bound-to-quasibound* [1] quantum well by placing the first excited state exactly at the well top as shown in Fig. 1. Dropping the first excited state to the well top causes the barrier to thermionic emission (roughly the energy height from the ground state to the well top) to be ~ 10 meV more in our bound-to-quasibound QWIP than in the bound-to-continuum one, theoretically causing the dark current to drop by a factor of ~ 6 at a temperature of 70 K [2,3]. The dark current as a function of temperature of the 8.5 μm peaked bound-to-quasibound QWIP is shown in Fig. 2. This compares well with the factor of ~ 4 drop we experimentally observe compared to the bound-to-continuum QWIP having the same peak wavelength.

2. TEST STRUCTURE RESULTS

Each period of the multi-quantum well (MQW) structure consists of a 45 \AA well of GaAs (doped $n = 5 \times 10^{17} \text{ cm}^{-3}$) and a 500 \AA barrier of $\text{Al}_{0.3}\text{Ga}_{0.7}\text{As}$. Stacking many identical quantum wells (typically 50) together increases photon absorption. Ground state electrons are provided in the detector by doping the GaAs well layers with Si. This photosensitive MQW structure is sandwiched between 0.5 μm GaAs top and bottom contact layers doped $n = 5 \times 10^{17} \text{ cm}^{-3}$, grown on a semi-insulating GaAs substrate by molecular beam epitaxy (MBE). Then a 0.7 μm thick GaAs cap layer on top of a 300 \AA $\text{Al}_{0.3}\text{Ga}_{0.7}\text{As}$ stop-etch layer was grown *in situ* on top of the device structure to fabricate the light coupling optical cavity. The MBE grown material was tested for absorption efficiency using a Fourier Transform Infrared (FTIR) spectrometer. Figure 3 shows the measured absorption quantum efficiency of this material at room temperature. The epitaxially grown material was processed into 200 μm diameter mesa test structures (area = $3.14 \times 10^{-4} \text{ cm}^2$) using wet chemical etching, and Au/Ge ohmic contacts were evaporated onto the top and bottom contact layers.

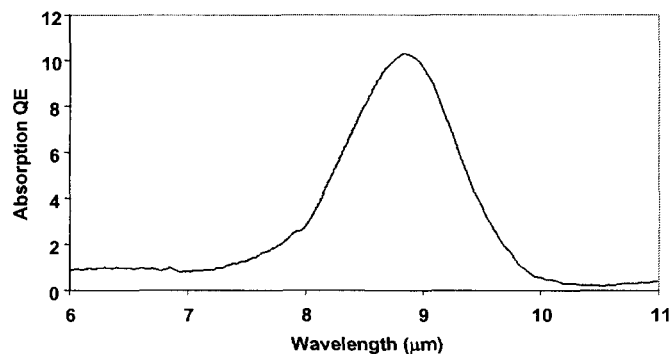


Fig. 3: Absorption quantum efficiency of the QWIP material at room temperature.

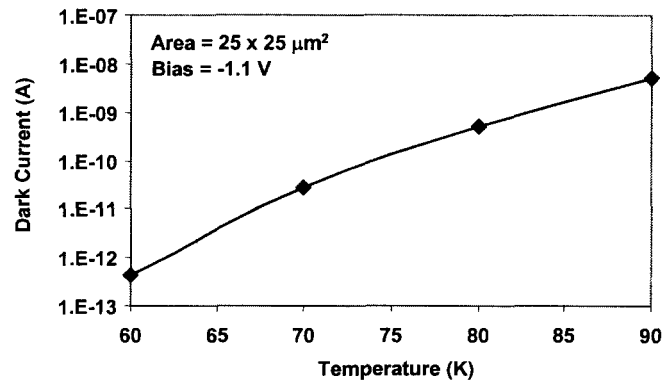


Fig. 2: Dark current of 8.5 μm peaked bound-to-quasibound QWIP as a function of temperature. Data were taken with a 200 μm diameter test structure and normalized to $25 \times 25 \mu\text{m}^2$ pixel.

The detectors were back illuminated through a 45° polished facet [5] and a responsivity spectrum is shown in Fig. 4. The responsivity of the detector peaks at 8.5 μm and the peak responsivity (R_p) of the detector is 83 mA/W at bias $V_B = -1.1$ V. The spectral width and the cutoff wavelength are $\Delta\lambda/\lambda = 10\%$ and $\lambda_c = 8.9 \mu\text{m}$ respectively. The measured absolute peak responsivity of the detector is small, up to about $V_B = -0.5$ V. Beyond that it increases nearly linearly with bias reaching $R_p = 420$ mA/W at $V_B = -5$ V. This type of behavior of responsivity versus bias is typical for a bound-to-quasibound QWIP. The peak quantum efficiency was 1.4% at bias $V_B = -1.1$ V for a 45°

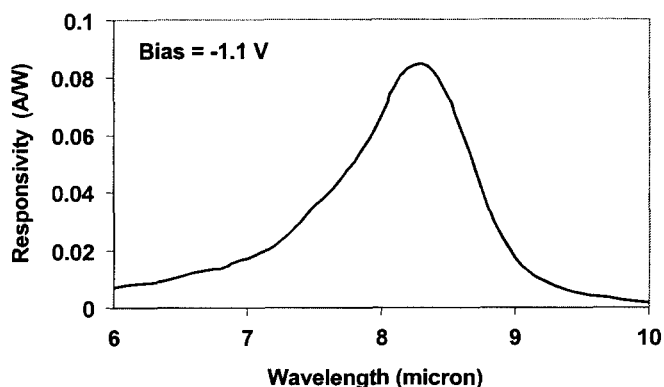


Fig. 4: Responsivity spectrum of a bound-to-quasibound LWIR QWIP test structure at temperature $T = 77$ K. The spectral response peak is at $8.5 \mu\text{m}$ and the long wavelength cutoff is at $8.9 \mu\text{m}$.

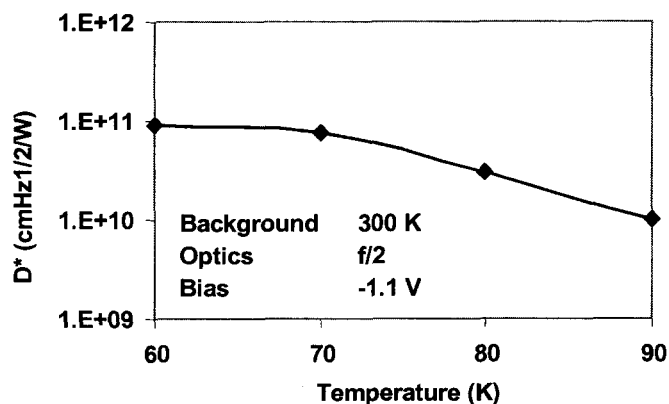


Fig. 5: Detectivity as a function of temperatures at bias of 1.2 V.

double pass. The lower quantum efficiency is due to the lower photoconductive gain at lower operating bias. Lower operating bias suppress the dark current. Due to lower readout multiplexer well depth (i.e., 11×10^6 electrons) a lower dark current is mandatory to achieve a higher operating temperature and longer integration times. In background limited performance (BLIP) condition the noise equivalent temperature difference (NETD) improves with the increasing integration time. In this case, the highest operating temperature of 65 K was determined by the cooling capacity of the small Sterling cooler used in an Indigo Phoenix™ camera.

The photoconductive gain g was experimentally determined using [8] $g = i_n^2 / 4eI_D B + 1/2N$, where B is the measurement bandwidth, N is the number of quantum wells, and i_n is the current noise, which was measured using a spectrum analyzer. The photoconductive gain of the detector reached 0.98 at $V_B = -5$ V. Since the gain of QWIP is inversely proportional to the number of quantum wells N , the better comparison would be the well capture probability p_c , which is directly related to the gain [8] by $g = 1/Np_c$. The calculated well capture probabilities are 25% at low bias (i.e., $V_B = -1$ V) and 2% at high bias (i.e., $V_B = -5$ V) which together indicate the excellent hot-electron transport in this device structure. The peak detectivity is defined as $D_p^* = R_p \sqrt{AB} / i_n$, where R_p is the peak responsivity, A is the area of the detector and $A = 3.14 \times 10^{-4} \text{ cm}^2$. The measured peak detectivity at bias $V_B = -1.2$ V and temperature $T = 65$ K is $1 \times 10^{11} \text{ cm}\sqrt{\text{Hz}}/\text{W}$. Figure 5 shows the bias dependence of peak detectivity as a function of temperature. These detectors show BLIP at bias $V_B = -2$ V and temperature $T = 72$ K for 300 K background with $f/2$ optics.

3. 640x512 FORMAT FOCAL PLANES

Although random reflectors have achieved relatively high quantum efficiencies with large test device structures, it is not possible to achieve the similar high quantum efficiencies with random reflectors on small focal plane array pixels due to the reduced width-to-height aspect ratios. In addition, it is difficult to fabricate random reflectors for shorter wavelength detectors relative to very long-wavelength detectors (i.e., $15 \mu\text{m}$) due to the fact that feature sizes of random reflectors are linearly proportional to the peak wavelength of the detectors. For example, the minimum feature size of the random reflectors of $15 \mu\text{m}$ cutoff and $9 \mu\text{m}$ cutoff FPAs were 1.25 and $0.6 \mu\text{m}$ respectively and it is difficult to fabricate sub-micron features by contact photolithography. As a result, the random reflectors of the $9 \mu\text{m}$ cutoff FPA were less sharp and had fewer scattering centers compared to the random reflectors of the $15 \mu\text{m}$ cutoff QWIP FPA. It is well known that QWIPs do not absorb radiation incident normal to the surface unless the IR radiation has an electric field component normal to the layers of superlattice (growth direction) [5]. As we have discussed before [5,6], more IR light can be coupled to the QWIP detector structure by incorporating a two dimensional grating surface on top of the detectors which also removes the light coupling limitations and makes two dimensional QWIP imaging arrays feasible. This two dimensional grating structure was fabricated on the detectors by using standard photolithography and CCl_2F_2 selective dry etching.

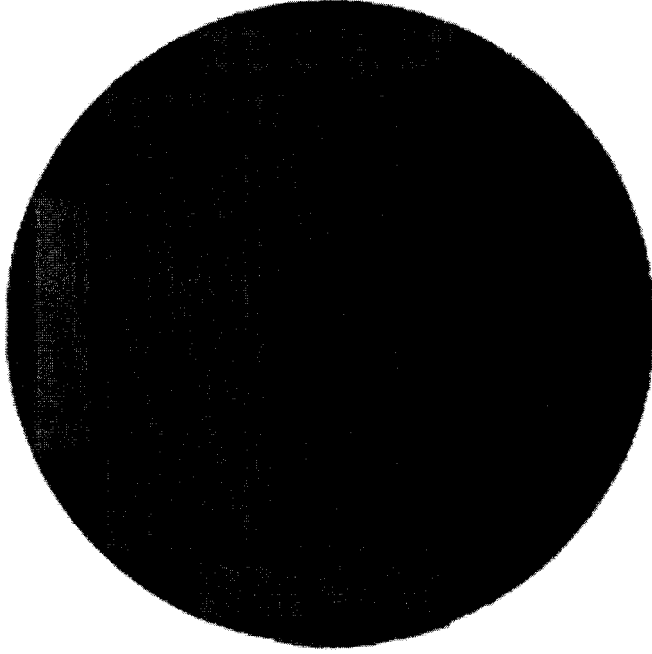


Fig 6. Twelve 640x512 QWIP focal plane arrays on a 3 inch GaAs wafer.

After the 2-D grating array was defined by the lithography and dry etching, the photoconductive QWIPs of the 640x512 FPAs were fabricated by wet chemical etching through the photosensitive GaAs/Al_xGa_{1-x}As multi-quantum well layers into the 0.5 μm thick doped GaAs bottom contact layer. The pitch of the FPA is 25 μm and the actual pixel size is 23x23 μm². The 2-D gratings on top of the detectors were then covered with Au/Ge and Au for Ohmic contact and reflection. Figure 6 shows twelve processed QWIP FPAs on a 3 inch GaAs wafer. Indium bumps were then evaporated on top of the detectors for Si readout circuit (ROC) hybridization. A single QWIP FPA was chosen and hybridized (via indium bump-bonding process) to a 640x512 CMOS multiplexer (ISC 9803) and biased at V_B = -1.2 V. At temperatures below 72 K, the signal to noise ratio of the system is limited by array non-uniformity, multiplexer readout noise, and photo current (photon flux) noise. At temperatures above 72 K, temporal noise due to the QWIP's higher dark current becomes the limitation. As mentioned earlier this higher dark current is due to thermionic emission and thus causes the charge storage capacitors of the readout circuitry to saturate. Since the QWIP is a high impedance device, it should yield a

very high charge injection coupling efficiency into the integration capacitor of the multiplexer. In fact Bethea *et al.* [2] have demonstrated charge injection efficiencies approaching 90%. Charge injection efficiency can be obtained from [3].

$$\eta_{inj} = \frac{g_m R_{Det}}{1 + g_m R_{Det}} \left[\frac{1}{1 + \frac{j\omega C_{Det} R_{Det}}{1 + g_m R_{Det}}} \right] \quad (1)$$

where g_m is the transconductance of the MOSFET and it is given by $g_m = eI_{Det}/kT$. The differential resistance R_{Det} of the pixels at -1.2 V bias is 4.3×10^{10} Ohms at $T = 65$ K and detector capacitance C_{Det} is 3.0×10^{-14} F. The detector dark current $I_{Det} = 1.5$ pA under the same operating conditions. According to equation (1) the charge injection efficiency $\eta_{inj} = 90\%$ at a frame rate of 30 Hz. The FPA was back-illuminated through the flat thinned substrate membrane (thickness ≈ 1300 Å). This initial array gave excellent images with 99.92% of the pixels working (number of dead pixels ≈ 250), demonstrating the high yield of GaAs technology. The operability was defined as the percentage of pixels having noise equivalent differential temperature less than 100 mK at 300 K background and in this case operability happens to be equal to the pixel yield.

We have used the following equation to calculate the noise equivalent temperature difference NETD of the FPA.

$$NETD = \frac{\sqrt{AB}}{D_B^* (dP_B / dT) \sin^2(\theta/2)} \quad (2)$$

where D_B^* is the blackbody detectivity, dP_B/dT is the derivative of the integrated blackbody power with respect to temperature, and θ is the field of view angle [i.e., $\sin^2(\theta/2) = (4f^2+1)^{-1}$, where f is the f number of the optical system]. Figure 7 shows the NETD of the FPA estimated from test structure data as a function of temperature for bias voltages $V_B = -1.2$ V. The background temperature $T_B = 300$ K, the area of the pixel $A = (23 \mu m)^2$, the f number of the optical system

is 2, and the frame rate is 30 Hz. Figure 8 shows the measured NETD of the FPA at an operating temperature of $T = 65$ K, 16 msec integration time, bias $V_B = -1.2$ V for 300 K background with $f/2$ optics and the mean value is 29 mK. This agrees reasonably with our estimated value of 10 mK based on test structure data. The net peak quantum efficiency of the FPA was 1.4% (lower focal plane array quantum efficiency is attributed to lower photoconductive gain at lower operating bias) and this corresponds to an average of three passes of IR radiation (equivalent to a single 45° pass) through the photosensitive multi-quantum well region. It is worth noting that under BLIP condition the performance of the detectors is independent of the photoconductive gain, and it depends only on the absorption quantum efficiency.

4. 640x512 PIXEL HAND-HELD CAMERA

A 640x512 QWIP FPA hybrid was mounted onto a 330 mW integral Sterling closed-cycle cooler assembly and installed into an Indigo Phoenix™ camera-body, to demonstrate a hand-held LWIR camera (shown in Fig. 9). The Phoenix™ infrared camera system has been developed by Indigo Systems Corporation to meet the needs of the research, industrial and ruggedized OEM communities. The system is comprised of a camera head and a selection of two video processing back ends. The camera head was made of Indigo's standard 640x512 format readout ISC 9803, mated to a long-wavelength QWIP detector materials. Two video processing units are the Real Time Imaging Electronics (RTIE) that provide conventional NTSC video as well as corrected parallel digital video out at video rates and the Digital Acquisition System (DAS) that provides high-speed (40 MHz) raw digital data acquisition and output with limited real time video for system setup and focusing. The other element of the camera is a 100 mm focal length germanium lens, with a 5.5 degree field of view. It is designed to be transparent in the 7-14 μm wavelength range, to be compatible with the QWIP's 8.5 μm operation. The digital acquisition resolution of the camera is 14-bits, which determines the instantaneous dynamic range of the camera (i.e., 16,384). However, the dynamic range of QWIP is 85 Decibels. Its nominal power consumption is less than 45 Watts.

The preliminary data taken from a test set up has shown mean NETD of 29 mK (the higher NETD is due to the 65% transmission through the lens assembly, and system noise of the measurement set up) at an operating temperature of $T = 65$ K and bias $V_B = -1.2$ V, for a 300 K background. The uncorrected photocurrent non-uniformity (which includes a 1% non-uniformity of the ROC and a 1.4% non-uniformity due to the cold-stop in front of the FPA not yielding the same field of view to all the pixels) of the 327,680 pixels of the 640x512 FPA is about 14% (= σ/mean). The non-uniformity after two-point (17° and 27° Celsius) correction improves to an impressive 0.3%. It is worth noting that these

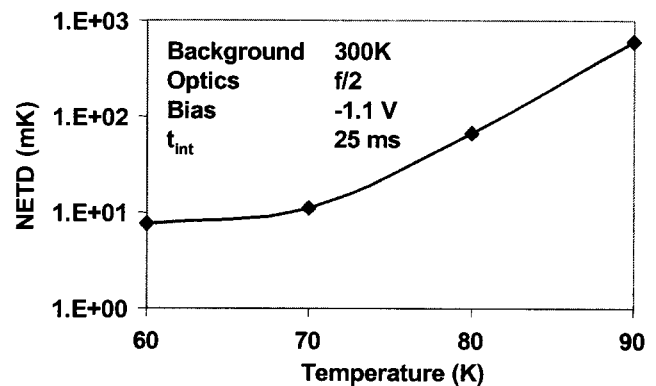


Fig. 7: Noise equivalent temperature difference NETD estimated from test structure data as a function of temperature for bias voltage $V_B = -1.2$ V. The background temperature $T_B = 300$ K and the area of the pixel $A = (23 \mu\text{m})^2$.

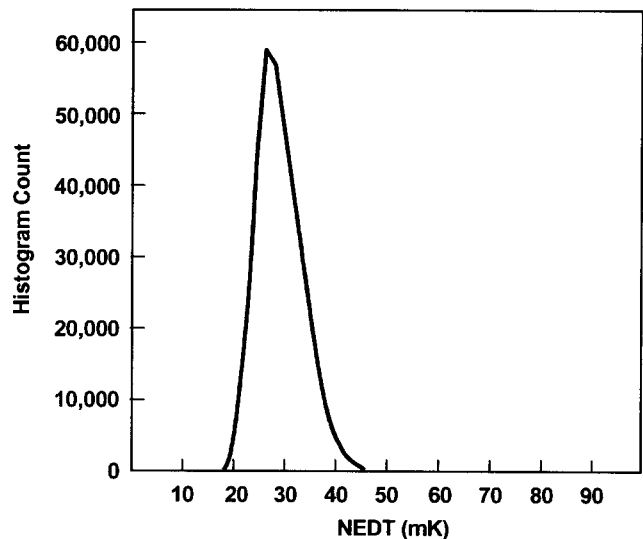


Fig. 8: NETD histogram of the 327,680 pixels of the 640x512 array showing a high uniformity of the FPA. The uncorrected non-uniformity (= standard deviation/mean) of the FPA is only 14% including 1% non-uniformity of ROC and 1.4% non-uniformity due to the cold-stop not being able to give the same field of view to all the pixels in the FPA.

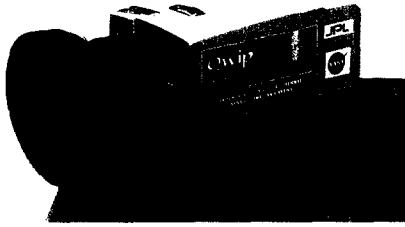


Fig. 9: Picture of the 640x512 hand-held long wavelength QWIP camera (QWIP Phoenix™).



Fig. 10: One frame of video image taken with the 9 μm cutoff 640x512 pixel QWIP Phoenix™ camera.

data were taken from the first 640x512 QWIP FPA which we produced. Thus, we believe that there is a plenty of room for further improvements of these FPA.

Video images were taken at a frame rate of 30 Hz at temperatures as high as $T = 70$ K, using a ROC capacitor having a charge capacity of 11×10^6 electrons (the maximum number of photoelectrons and dark electrons that can be counted in the time taken to read each detector pixel). Figure 10 shows one frame of a video image taken with a 9 μm cutoff 640x512 pixel QWIP Phoenix™ camera.

It should be noted that these initial unoptimized FPA results are far from optimum. The focal plane array performance data reported in this paper was taken with a laboratory measurement set up. Estimates based on the single pixel data show that these FPAs should be able to provide 7 mK NETD with 30 msec integration time, which can be achieved at 1.1V bias. Focal planes are now being integrated with the close cycle stirling coolers. Then, these FPA/dewar assemblies will be integrated with Phoenix™ camera electronics. Thus, we expect QWIP Phoenix™ camera to achieve the performance of NETD < 20 mK with shorter integration time (< 16 msec with high bias), and the performance of NETD < 10 mK with longer integration time at 30 Hz (30 msec integration with low bias).

5. 640x512 PIXEL FOUR-COLOR SPATIALLY SEPARATED FOCAL PLANE ARRAY

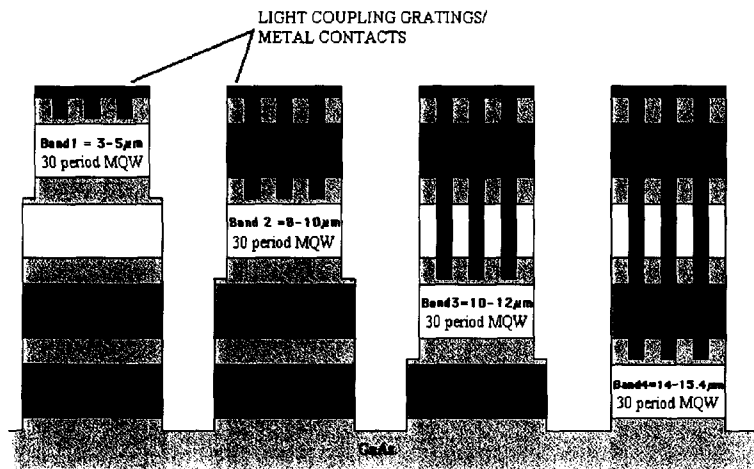


Fig. 11: Layer diagram of four-band QWIP device structure and the deep groove 2-D periodic grating structure. Each pixel represent a 640x128 pixel area of the four-band focal plane array.

One unique feature of this spatially separated four-band focal plane array is that the four infrared bands are independently readable on a single imaging array. This feature leads to a reduction in instrument size, weight, mechanical complexity, optical complexity and power requirements since no moving parts are needed. Furthermore, a single optical train can be employed, and the focal plane can operate at a single temperature.

This four-band device structure was achieved by the growth of multi stack QWIP structures separated by heavily doped contact layers, on a GaAs substrate. Device parameters of each QWIP stack were designed to respond in different wavelength bands. Figure 11 shows the schematic device structure of a four color QWIP imager. A typical QWIP stack consists of a MQW structure of GaAs quantum wells separated by Al_xGa_{1-x} As barriers. The actual

device structure consists of a 15 period stack of 3-5 μm QWIP structure, a 25 period stack of 8.5-10 μm QWIP structure, a 25 period stack of 10-12 μm QWIP structure and a 30 period stack of 13-15.5 μm QWIP structure. Each photosensitive MQW stack was separated by a heavily doped (thickness 0.2 to 0.8 μm) intermediate GaAs contact layer (see Figure 11). Since the dark current of this device structure is dominated by the longest wavelength portion of the device structure, the VLWIR QWIP structure has been designed to have a bound-to-quasibound intersubband absorption peak at 14.0 μm . Other QWIP device structures have been designed to have a bound-to-continuum intersubband absorption process, because the photo current and dark current of these devices are relatively small compared to the VLWIR device. This whole four-band QWIP device structure was then sandwiched between 0.5 μm GaAs top and bottom contact layers doped with $n = 5 \times 10^{17} \text{ cm}^{-3}$, and was grown on a semi-insulating GaAs substrate by MBE.

The individual pixels were defined by photolithographic processing techniques (masking, etching, chemical vapor deposition, metal deposition, etc.). Four separate detector bands were defined by a deep trench etch process and the unwanted spectral bands were eliminated by a detector short-circuiting process. The unwanted top detectors were electrically shorted by a gold coated reflective 2-D etch gratings as shown in the Fig. 11. In addition to shorting, these gratings serve as light couplers for active QWIP stack in each detector pixel. Design and optimization of these 2-D gratings to maximize QWIP light coupling were extensively discussed in reference 5. The unwanted bottom detectors were electrically shorted at the end of each detector pixel row.

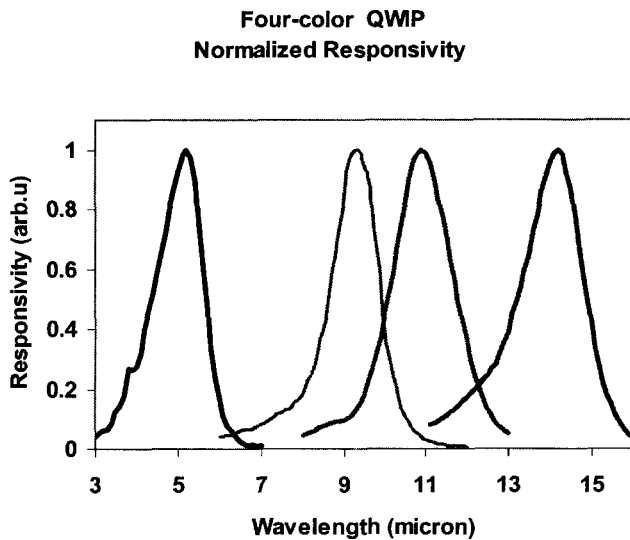


Fig. 12: Normalized spectral response of the four-band QWIP focal plane array.

Typically, in single-band QWIP FPAs, quarter wavelength deep ($h = \lambda_p/4n_{\text{GaAs}}$) grating grooves are used for efficient light coupling. However, in the four-band FPA, the thickness of the quarter wavelength deep grating grooves are not deep enough to short circuit the top three MQW QWIP stacks (e.g.: three top QWIP stacks on 14-15.5 μm QWIP in Fig. 11). Thus, three-quarter wavelength groove depth 2-D gratings ($h = 3\lambda_p/4n_{\text{GaAs}}$) were used to short the top unwanted detectors over the 10-12 and 14-15.5 microns bands. This technique optimized the light coupling to each QWIP stack at corresponding bands while keeping the pixel (or mesa) height at the same level which is essential for indium bump-bonding process used for detector array and readout multiplexer hybridization. Figure 12 shows the normalized spectral responsivities of all four spectral bands of this four-band focal plane array.

noise ratio of the 4-5 μm spectral band is limited by array non-uniformity, multiplexer readout noise, and photo current (photon flux) noise. At temperatures above 45 K, temporal noise due to the 14-15.5 μm QWIP's higher dark current becomes the limitation. The 8-10 and 10-12 μm spectral bands have shown BLIP performance at temperatures between 45 and 83 K. The FPAs were back-illuminated through the flat thinned substrate membrane (thickness $\approx 1300 \text{ \AA}$). This initial array gave excellent images with 99.9% of the pixels working (number of dead pixels ≈ 250), demonstrating the high yield of GaAs technology. The operability was defined as the percentage of pixels having noise equivalent differential temperature less than 100 mK at 300 K background and in this case operability happens to be equal to the pixel yield.

Few QWIP FPAs were chosen and hybridized to a 640x512 CMOS multiplexer (ISC 9803) and biased at $V_B = -1.1 \text{ V}$. At temperatures below 83 K, the signal to

A 640x512 pixel four-band QWIP FPA hybrid was mounted onto a 84-pin lead-less chip carrier and installed into a laboratory dewar which is cooled by liquid helium to demonstrate a 4-band simultaneous imaging camera. The FPA was cooled to 45 K and the temperature was stabilized by regulating the pressure of gaseous helium. The other element of the camera is a 100 mm focal length AR coated germanium lens, which gives a $9.2^\circ \times 6.9^\circ$ field of view. It is designed to

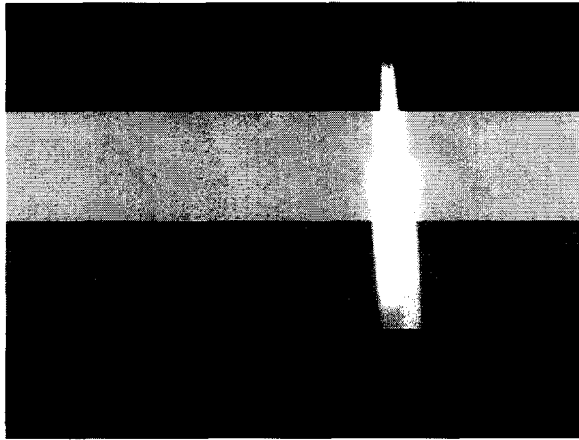


Fig. 13: One frame of video image taken with the 4-15.5 microns cutoff four-band 640x512 pixel QWIP camera. The image is barely visible in the 14-15.5 microns spectral band due to the poor optical transmission of the anti-reflection layer coated germanium lens.

by the quantum well width (L_w) and the barrier height, i.e. the Al mole fraction (x) of the barrier. Since each single set of parameters for a bound-to-quasibound quantum well⁴ corresponds to a spectral band pass of about $1.5 \mu\text{m}$, three different sets of values are sufficient to cover a $10\text{-}16 \mu\text{m}$ spectral region. The MQW structure consists of many periods of these three-quantum-well units separated by thick barriers.

The device structure reported here involved 33 repeated layers of GaAs three-quantum-well units separated by $L_B \sim 575 \text{ \AA}$ thick $\text{Al}_x\text{Ga}_{1-x}\text{As}$ barriers. The well thickness of the quantum wells of three-quantum-well units are designed to respond at peak wavelengths around $13, 14, \text{ and } 15 \mu\text{m}$ respectively. These wells are separated by $L_u \sim 75 \text{ \AA}$ thick $\text{Al}_x\text{Ga}_{1-x}\text{As}$ barriers. The Al mole fraction (x) of barriers throughout the structure was chosen such that the $\lambda_p = 13 \mu\text{m}$ quantum well operates under bound-to-quasibound conditions. The excited state energy level broadening has been further enhanced due to the overlap of the wavefunctions associated with excited states of quantum wells separated by thin barriers. Energy band calculations based on a two band model show excited state energy levels spreading about 28 meV .

The sample was grown on a semi-insulating 3-inch GaAs substrate by molecular beam epitaxy. It consists of the device structure described above sandwiched between top and bottom contact layers. Transport carriers (electrons) were provided by doping all GaAs wells and contact layers with Si. In order to measure dark current-temperature curve, spectral responsivity (see Figure 14-16) and noise, $200 \mu\text{m}$ diameter mesas were fabricated using wet chemical etching and Au/Ge ohmic contacts were evaporated onto the top and bottom contact layers.

The responsivity spectra of these detectors were measured using a 1000 K blackbody source and a grating monochromator. The detectors were back illuminated through a 45° polished facet to obtain normalized responsivity spectra at different bias voltages. Then the absolute spectral responsivities were obtained by measuring total photocurrent from a calibrated black-body source. In Fig. 15, responsivity curve at $V_B = -2.5 \text{ V}$ bias voltage shows broadening of the spectral response up to $\Delta\lambda \sim 5.5 \mu\text{m}$, i.e. the full width at half maximum from $10.5 - 16 \mu\text{m}$. This broadening $\Delta\lambda/\lambda_p \sim 42 \%$ is about a 400% increase compared to a typical bound-to-quasibound QWIP.

Unlike narrow-band QWIPs, these detectors show spectral peak shifts from $\lambda = 11.5 \mu\text{m}$ to $\lambda = 15.1 \mu\text{m}$ as negative bias voltage increased from $V_B = -1 \text{ V}$ to $V_B = -5 \text{ V}$ and similar behavior ($\lambda = 11.5 \mu\text{m}$ to $\lambda = 14.7 \mu\text{m}$ for $V_B = +1 \text{ V}$ to $V_B = +5 \text{ V}$) was observed under positive bias voltages as well. This suggests that there is no substantial carrier depletion due

be transparent in the $8\text{-}12 \mu\text{m}$ wavelength range. SEIRTM image processing station was used to obtain clock signals for readout multiplexer and to perform digital data acquisition and non-uniformity corrections. The digital data acquisition resolution of the camera is 14-bits, which determines the instantaneous dynamic range of the camera (i.e., 16,384), however, the dynamic range of QWIP is 85 Decibels. Video images were taken at a frame rate of 30 Hz at temperatures as high as $T = 45 \text{ K}$, using a ROC capacitor having a charge capacity of 11×10^6 electrons (the maximum number of photoelectrons and dark electrons that can be counted in the time taken to read each detector pixel). Figure 13 shows one frame of a video image taken with four-band 640×512 pixel QWIP camera.

6. 640X512 PIXEL BROAD-BAND QWIP IMAGING CAMERA

Broadband QWIP device structure is designed by repeating a unit of several quantum wells with slightly different parameters such as well width and barrier height²⁷. The positions of ground and excited states of the quantum well are determined

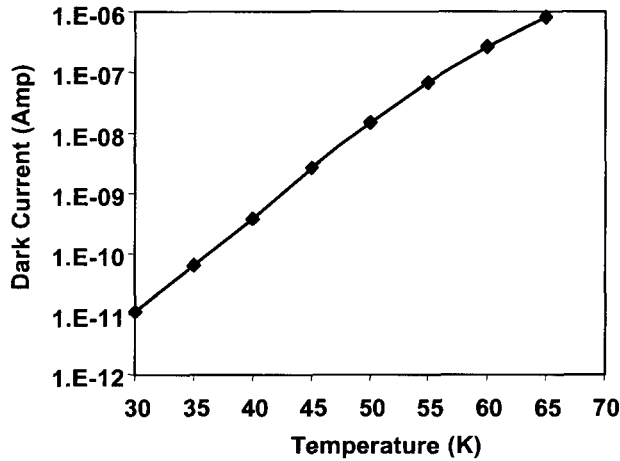


Fig. 14: Dark current-temperature curve of 10-15.4 μm broadband QWIP at bias $V_B = -2.5\text{V}$. Data were taken with a 200 μm diameter test structure and normalized to $25 \times 25 \mu\text{m}^2$ pixel.

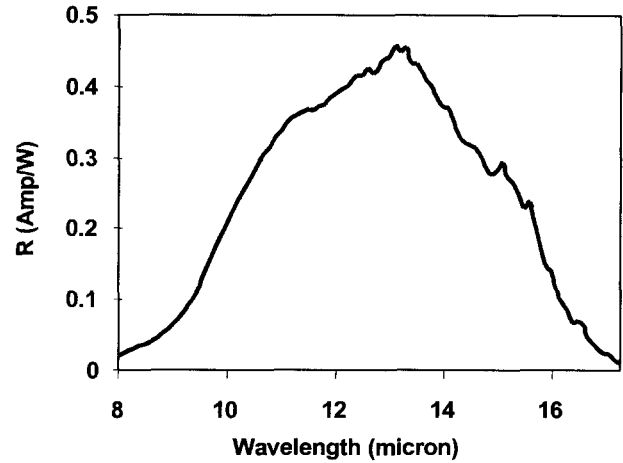


Fig. 15: Responsivity spectrum of a broadband QWIP test structure at temperature $T = 55\text{K}$. The spectral response peak is at 13.5 μm and the long wavelength cutoff is at 15.4 μm .

to the applied electric field within the three-quantum-units because the direction of peak shift remains the same under both positive and negative biases. The responsivity of the detector peaks at 13.5 μm and the peak responsivity (R_p) of the detector is 250 mA/W at bias $V_B = -2.5\text{V}$. The bias dependent peak responsivity of the detector is shown in Fig. 16. The measured absolute peak responsivity of the detector is small, up to about $V_B = -0.5\text{V}$. Beyond that it increases nearly linearly with bias reaching $R_p = 580\text{mA/W}$ at $V_B = -3.5\text{V}$. This type of behavior of responsivity versus bias is typical for a bound-to-quasibound QWIP. The peak quantum efficiency was 11% at bias $V_B = -2.5\text{V}$ for a 45° double pass. The lower quantum efficiency is due to the lower well doping density ($2 \times 10^{17}\text{cm}^{-3}$) as it is necessary to suppress the dark current at the highest possible operating temperature. A peak quantum efficiency as high as 25% has already been achieved with regular well doping density (i.e., $1 \times 10^{18}\text{cm}^{-3}$). Due to lower readout multiplexer well depth (i.e., 11×10^6 electrons) a lower dark current is mandatory to achieve a higher operating temperature. In this case, the highest operating temperature of 45 K was determined by the well depth of the readout multiplexer.

The dark current noise i_n of the device was measured using a spectrum analyzer at $T = 55\text{K}$ as a function of bias voltage. The noise gain g_n can now be obtained using the g-r noise calculated based on standard noise expression:

$i_n = \sqrt{4eI_d g_n \Delta B}$ where I_d is the dark current and ΔB is the bandwidth. Using experimental measurements of noise and

responsivity, one can now calculate specific detectivity D^* from $D^* = R\sqrt{A\Delta f} / i_n$, where A is area of the detector.

Calculated D^* value for the present device ($\lambda = 15.4\text{ }\mu\text{m}$) at $T = 55\text{K}$, and $V_B = 2.5\text{V}$ is $3 \times 10^{10}\text{ cm}\sqrt{\text{Hz}}/\text{W}$. Even with broader response, this D^* is comparable to previously reported D^* of QWIPs with narrow spectral response. Figures 17 and 18 show the detectivity D^* and the noise equivalent temperature difference (NEAT) as a function of the operating temperature of the device.

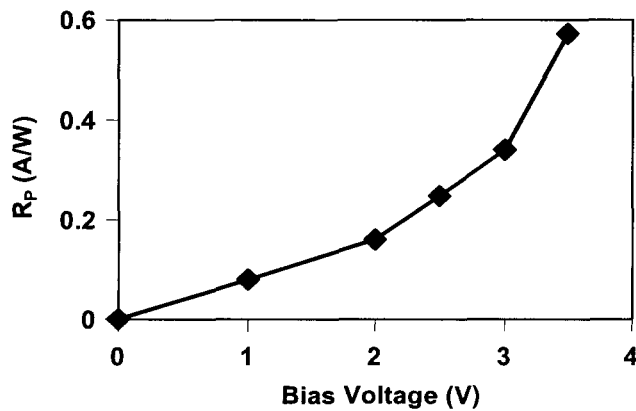


Fig. 16: Peak responsivity as a function of bias voltage at temperature $T = 55\text{K}$.

It is well known that QWIPs do not absorb radiation incident normal to the surface unless the IR radiation have an electric field component normal to the layers of

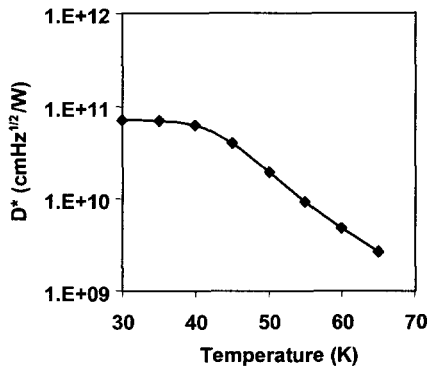


Fig. 17: Detectivity as a function of temperatures at bias voltage $V_B = -2.5V$.

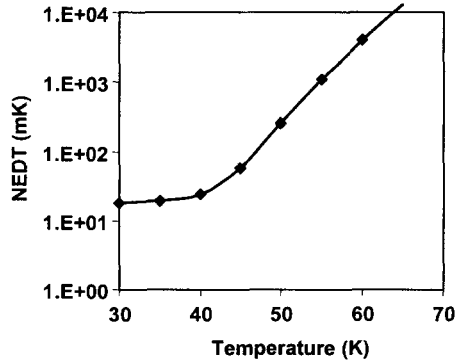


Fig. 18: Noise equivalent temperature difference as a function of temperatures at bias voltage $V_B = -2.5V$.

superlattice (growth direction). As discussed elsewhere many more passes of IR light inside the detector structure can be obtained by incorporating a randomly roughened reflecting surface on top of the detectors which also removes the light coupling limitations and makes two dimensional QWIP imaging arrays feasible. This random structure was fabricated on the detectors by using standard photolithography and CCl_2F_2 selective dry

etching. The advantage of the photolithographic process over a completely random process is the ability to accurately control the feature size and preserve the pixel to pixel uniformity which is a prerequisite for high sensitivity imaging FPAs.

After the random reflector array was defined by the lithography and dry etching, the photoconductive QWIPs of the 640x512 FPAs were fabricated by dry etching through the photosensitive GaAs/ $Al_xGa_{1-x}As$ multi-quantum well layers into the 0.5 μm thick doped GaAs bottom contact layer. The pitch of the FPA is 25 μm and the actual pixel size is 23x23 μm^2 . The random reflectors on top of the detectors were then covered with Au/Ge and Au for Ohmic contact and reflection. Indium bumps were then evaporated on top of the detectors for Si readout circuit (ROC) hybridization. A single QWIP FPA was chosen and hybridized (via indium bump-bonding process) to a 640x512 CMOS multiplexer (Indigo Systems 9803) and biased at $V_B = -2.5 V$. At temperatures below 48 K, the signal to noise ratio of the system is limited by array non-uniformity, multiplexer readout noise, and photo current (photon flux) noise (see Figure 19). At

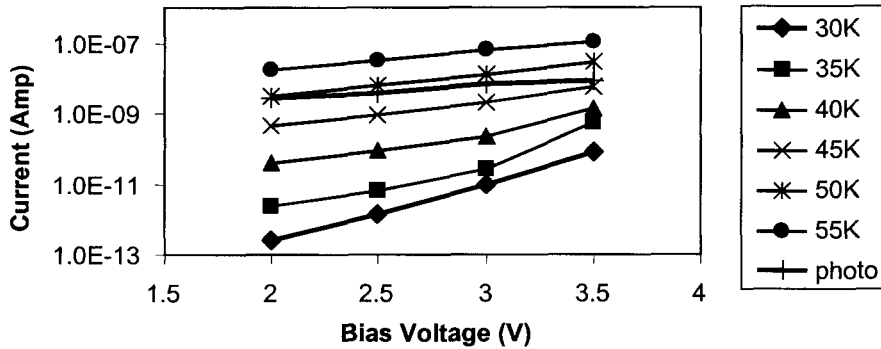


Fig. 19: Dark current and the photo current of 10-15.4 μm broadband QWIP as a function of bias voltage.

temperatures above 48 K, temporal noise due to the QWIP's higher dark current becomes the limitation. As mentioned earlier this higher dark current is due to thermionic emission and thus causes the charge storage capacitors of the readout circuitry to saturate. Since the QWIP is a high impedance device, it should yield a very high charge injection coupling efficiency into the integration capacitor of the multiplexer. In fact Bethea *et al.*⁸ have demonstrated charge injection efficiencies approaching 90%.

Charge injection efficiency can be obtained from equation (1), where g_m is the transconductance of the MOSFET and is given by $g_m = eI_{Det}/kT$. The differential resistance R_{Det} of the pixels at -2 V bias is 5.4×10^{10} Ohms at $T=45 K$ and detector capacitance C_{Det} is 1.4×10^{-14} F. The detector dark current $I_{Det} = 8$ pA under the same operating conditions. According to equation (1) the charge injection efficiency $\eta_{inj} = 99.5\%$ at a frame rate of 30 Hz. The FPA was back-illuminated through the flat thinned substrate membrane (thickness $\approx 1300 \text{ \AA}$). This thinned GaAs FPA membrane has completely eliminated the thermal mismatch between the silicon CMOS readout multiplexer and the GaAs based QWIP FPA. Basically, the thinned GaAs based QWIP FPA membrane adapts to the thermal expansion and contraction

coefficients of the silicon readout multiplexer. Thus, thinning has played an extremely important role in the fabrication of large area FPA hybrids. In addition, this thinning has completely eliminated the pixel-to-pixel optical cross-talk of the FPA. This initial array gave very good images with 99.9% of the pixels working, demonstrating the high yield of GaAs technology. The operability was defined as the percentage of pixels having noise equivalent differential temperature less than 100 mK at 300 K background with $f/2$ optics and in this case operability happens to be equal to the pixel yield.

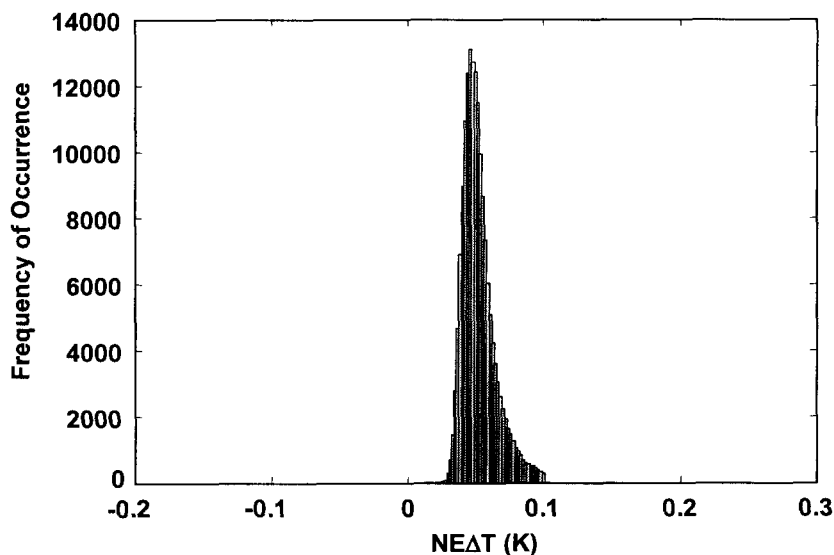


Fig. 20: Noise equivalent temperature difference (NEAT) histogram of the 327,680 pixels of the 640 x 512 array showing a high uniformity of the FPA. The uncorrected non-uniformity (= standard deviation/mean) of this unoptimized FPA is only 6.3% including 1% non-uniformity of ROC and 1.4% non-uniformity due to the cold-stop not being able to give the same field of view to all the pixels in the FPA.

We have used the equation (2) to calculate the NEAT of the FPA. where D_B^* is the blackbody detectivity, dP_B/dT is the derivative of the integrated blackbody power with respect to temperature, and θ is the field of view angle [i.e., $\sin^2(\theta/2) = (4f^2+1)^{-1}$, where f is the f number of the optical system]. The background temperature $T_B = 300$ K, the area of the pixel $A = (23 \mu\text{m})^2$, the f number of the optical system is 2, and the frame rate is 30 Hz. Figure 20 shows the experimentally measured NEAT histogram of the FPA at an operating temperature of $T = 35$ K, bias $V_B = -2.5$ V at 300 K background with $f/2$ optics and the mean value is 55 mK. This agrees reasonably well with our estimated value of 25 mK based on test structure data. The read noise of the multiplexer is 500 electrons. The factor of two shortfall of NEAT is mostly attributed to decrease in bias voltage across the detectors during charge accumulation (common in many direct injection type readout multi-

plexers) and read noise of the readout multiplexer. The experimentally measured peak quantum efficiency of the FPA was 9.5% which agrees well with the 11% quantum efficiency estimated from the single element detector data.

A 640x512 QWIP FPA hybrid was mounted onto a 84-pin lead-less chip carrier and installed into a laboratory dewar which is cooled by liquid neon to demonstrate a LWIR imaging camera (FPA was cooled to 35K). The other element of the camera is a 100 mm focal length AR coated germanium lens, which gives a $9.2^\circ \times 6.9^\circ$ field of view. It is designed to be transparent in the 8-12 μm wavelength range (which is not fully compatible with the 10-15 micron broadband QWIP array). An image processing station was used to obtain clock signals for readout multiplexer and to perform digital data acquisition and non-uniformity corrections. The digital data acquisition resolution of the camera is 14-bits, which determines the instantaneous dynamic range of the camera (i.e., 16,384), however, the dynamic range of QWIP is 85 Decibels.

The measured mean NEAT of the QWIP camera is 55 mK at an operating temperature of $T = 35$ K and bias $V_B = -2.5$ V at 300 K background with $f/2$ optics (see Fig. 20). This is in good agreement with expected focal plane array sensitivity due to the practical limitations on charge handling capacity of the multiplexer, read noise, bias voltage and operating temperature. The uncorrected NEAT non-uniformity (which includes a 1% non-uniformity of the ROC and a 1.4% non-uniformity due to the cold-stop in front of the FPA not yielding the same field of view to all the pixels) of the 327,680 pixels of the 640x512 FPA is about 6.3% (= σ/mean). The non-uniformity after two-point (17° and 27° Celsius) correction improves to an impressive 0.1%. As mentioned earlier, this high yield is due to the excellent GaAs growth uniformity and the mature GaAs processing technology. Video images were taken at a frame rate of 30 Hz at temperatures as high as $T = 35$ K using a ROC capacitor having a charge capacity of 11×10^6 electrons.

ACKNOWLEDGEMENTS

Authors are grateful to C. P. Bankston, M. Bothwell, T. N. Krabach, and P. J. Grunthaler for encouragement and support during the development and optimization of QWIP FPAs at Jet Propulsion Laboratory for various applications. The research described in this paper was performed by the Jet Propulsion Laboratory, California Institute of Technology, and was sponsored by the NASA code R Micro & Nano Technology Program.

REFERENCES

1. S. D. Gunapala, J. K. Liu, J. S. Park, T. L. Lin, and M. Sundaram "Infrared Radiation Detecting Device", US Patent No. 6,211,529.
2. Sarath D. Gunapala, John K. Liu, Jin S. Park, Mani Sundaram, Craig A. Shott, Ted Hoelter, True-Lon Lin, S. T. Massie, Paul D. Maker, Richard E. Muller, and Gabby Sarusi "9 μm Cutoff 256x256 GaAs/Al_xGa_{1-x}As Quantum Well Infrared Photodetector Hand-Held Camera", IEEE Trans. Electron Devices, **44**, pp. 51-57, 1997.
3. Sarath D. Gunapala, Sumith V. Bandara, John K. Liu, Winn Hong, Mani Sundaram, Paul D. Maker, Richard E. Muller, Craig A. Shott, and Ronald Carralejo, "Long-Wavelength 640x486 GaAs/Al_xGa_{1-x}As Quantum Well Infrared Photodetector Snap-shot Camera", IEEE Trans. Electron Devices, **45**, 1890 (1998).
4. W. Cabanski, R. Breiter, R. Koch, K. H. Mauk, W. Rode, J. Ziegler, H. Schneider, M. Walther, and R. Oelmaier, SPIE Vol. 4369, pp. 547-558 (2001).
5. S. D. Gunapala and S. V. Bandara, "Quantum Well Infrared Photodetector (QWIP) Focal Plane Arrays," Semiconductors and Semimetals, Vol. 62, 197-282, Academic Press, 1999.
6. S. D. Gunapala, S. V. Bandara, A. Singh, J. K. Liu, S. B. Rafol, E. M. Luong, J. M. Mumolo, N. Q. Tran, J. D. Vincent, C. A. Shott, J. Long, and P. D. LeVan, "640x486 Long-wavelength Two-color GaAs/AlGaAs Quantum Well Infrared Photodetector (QWIP) Focal Plane Array Camera" IEEE Trans. Electron Devices, **47**, pp. 963-971, 2000.
7. S. D. Gunapala, S. V. Bandara, J. K. Liu, E. M. Luong, N. Stetson, C. A. Shott, J. J. Bock, S. B. Rafol, J. M. Mumolo, and M. J. McKelvey, "Long-wavelength 256X256 GaAs/AlGaAs Quantum Well Infrared Photodetector (QWIP) Palm-size Camera" IEEE Trans. Electron Devices, **47**, pp. 326-332, 2000.
8. W. A. Beck, "Photoconductive gain and generation-recombination noise in multiple-quantum-well infrared detectors," Appl. Phys. Lett. , Vol. **63**, pp. 3589-3591, 1993.
9. S. D. Gunapala, S. V. Bandara, J. K. Liu, E. M. Luong, S. B. Rafol, J. M. Mumolo, D. Z. Ting, J. J. Bock, M. E. Ressler, M. W. Werner, P. D. LeVan, R. Chehayeb, C. A. Kukkonen, M. Levy, P. LeVan, and M. A. Fauci, "Infrared Physics & Technology, Vol. **42**, pp. 267-282, (2001).